Biomedical Signal Processing and Control 79 (2023) 104011

Contents lists available at ScienceDirect

Biomedical Signal Processing and Control

journal homepage: www.elsevier.com/locate/bspc

A morphology-based feature set for automated Amyotrophic Lateral Sclerosis diagnosis on surface electromyography

Margarida Antunes [a,*], Duarte Folgado [a,b], Marília Barandas [a,b], André Carreiro [a], Carla Quintão [b], Mamede de Carvalho [c,d], Hugo Gamboa [a,b]

[a] Associação Fraunhofer Portugal Research, Rua Alfredo Allen 455/461, Porto, 4200-135, Portugal
[b] LIBPhys (Laboratory for Instrumentation, Biomedical Engineering and Radiation Physics), NOVA School of Science and Technology, Campus de Caparica, 2829-516, Portugal
[c] Department of Neurosciences and Mental Health, Hospital de Santa Maria, Centro Hospitalar Universitário Lisboa-Norte, Lisbon, Portugal
[d] Instituto de Medicina Molecular, Faculdade de Medicina, Universidade de Lisboa, Lisbon, Portugal

ARTICLE INFO

Keywords:
Amyotrophic Lateral Sclerosis
Surface electromyography
Time series
Signal processing
Feature selection
Machine learning

ABSTRACT

Amyotrophic Lateral Sclerosis (ALS) is a fast-progressing disease with no cure. Nowadays, needle electromyography (nEMG) is the standard practice for electrodiagnosis of ALS. Surface electromyography (sEMG) is emerging as a more practical and less painful alternative to nEMG but still has analytical and technical challenges. The objective of this work was to study the feasibility of using a set of morphological features extracted from sEMG to support a machine learning pipeline for ALS diagnosis. We developed a novel feature set to characterize sEMG based on quantitative measurements to surface representation of Motor Unit Action Potentials. We conducted several experiments to study the relevance of the proposed feature set either individually or combined with conventional feature sets from temporal, statistical, spectral, and fractal domains. We validated the proposed machine learning pipeline on a dataset with sEMG upper limb muscle data from 17 ALS patients and 24 control subjects. The results support the utility of the proposed feature set, achieving an F_1 score of (81.9 ± 5.7) for the onset classification approach and (83.6 ± 6.9) for the subject classification approach, solely relying on features extracted from the proposed feature set in the right first dorsal interosseous muscle. We concluded that introducing the proposed feature set is relevant for automated ALS diagnosis since it increased the classifier performance during our experiments. The proposed feature set might also help design more interpretable classifiers as the features give additional information related to the nature of the disease, being inspired by the clinical interpretation of sEMG.

1. Introduction

Amyotrophic lateral sclerosis (ALS) is a chronic neurodegenerative disease that leads to muscle atrophy due to the progressive loss of motor neurons [1,2]. According to a review of epidemiological studies provided by [3], there has been an increasing number of patients diagnosed with ALS over the last years. There are two main disease phenotypes, spinal-onset and bulbar-onset, corresponding to weakness presentation in limbs an bulbar muscles, respectively [2,4]. Gradually, the condition of the patient deteriorates up to a severely disabled state, leading to an average survival from the onset of symptoms of approximately three years [4,5].

The most frequently performed exam as part of the diagnosis routine is electromyography (EMG), which measures the electric potentials generated by muscular cells. The MU, which represents the anatomical and functional element of the neuromuscular system [4], can be described as a single motor neuron and all of the muscle fibers that it innervates [1]. The electrical activity of the muscle fibers generates electrical changes called MUAPs, which are distinguishable in shape and size for each MU [6,7], as can be seen in Fig. 1.

The ALS diagnosis guidelines defined in 2008 during the Awaji consensus meeting support the utility of needle EMG (nEMG) as an attempt to improve the diagnostic accuracy of the Revised El Escorial criteria [8,9]. nEMG is an invasive technique that uses a needle recording electrode inserted directly into the muscle, providing accurate electrical potential measurements. However, this invasive technique has the disadvantage of being particularly painful for patients, which hinders its repetitive usage for tracking disease progression in routine medical appointments. Additionally, it cannot be performed in an outpatient setting since it requires professional expertise, and its

* Corresponding author.
E-mail address: maria.antunes@fraunhofer.pt (M. Antunes).

https://doi.org/10.1016/j.bspc.2022.104011
Received 21 February 2022; Received in revised form 12 May 2022; Accepted 11 July 2022
Available online 22 August 2022

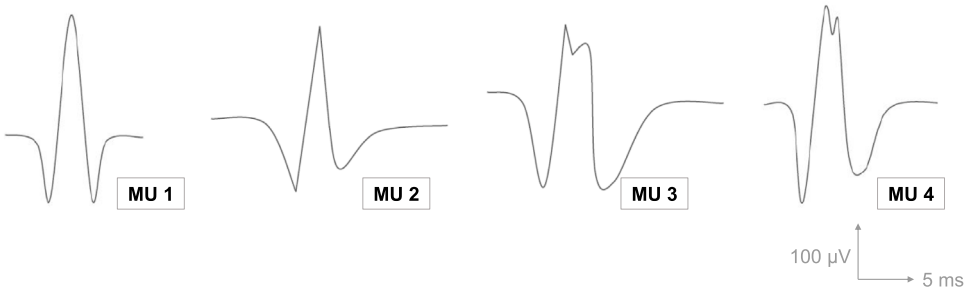

Fig. 1. Illustrative examples of different MUAP waveforms originated from different MUs.

recordings often present variability due to small movements of the electrodes with higher muscular force [6].

These are some of the reasons for the growing interest in surface EMG (sEMG) [10], a method that also measures the electrical activity of skeletal muscles, but it relies on surface electrodes. Despite the versatility of these electrodes, they record signals with a lower signal-to-noise ratio in comparison with nEMG, and the tissues underlying the electrodes act as a low-pass filter, causing similar shapes in potentials from different motor units [11]. Since surface electrodes are farther away from the muscle fibers, the recorded MUAPs are lower in amplitude and with higher superposition probability of multiple MUAPs. These drawbacks have resulted in the long medical community's discrediting of sEMG potential in clinical practice [12].

The latest technological advances in sensing hardware, computing capacity, and signal processing for sEMG have contributed to an increasingly acceptance of this technique in clinical practice. According to a recent systematic review [13], sEMG offers significant practical and analytical flexibility compared to nEMG due to its non-invasive nature, and there is a need for multi-disciplinary research collaboration on the topic. From these conclusions arises the need to understand the role and utility of sEMG in predicting the ALS diagnosis through Machine Learning (ML) models. This is of particular interest if relations can be established between the sEMG characteristics and the actual pathophysiology phenomena of the disease.

The interpretation of quantitative data from a sEMG signal can be very informative, namely through the use of time, frequency, and time–frequency features. For a thorough review of such features across different applications refer to [14–16]. Several works have been proposed in the context of ALS diagnosis using these features and automated learning architectures. The experimental data collection setup on these experiments is often categorized into nEMG, sEMG, and high-density surface electromyography (HDsEMG).

In the context of nEMG, statistical, temporal and spectral features have proven useful in discriminating the disease [17–20]. HDsEMG is a sEMG technique that uses arrays of individual electrodes designed to record simultaneously, thus increasing the spatial characterization of the electrical muscle activity. Some studies have addressed the potential advantages of this technique in identifying fasciculation potentials (FPs) [21,22] and used for ALS diagnosis [10].

The application of learning algorithms on sEMG data has a broad range application areas, such as assistive technology [23–25], rehabilitation technology [26], and silent speech recognition [27]. In the context of using sEMG for objective assessment of ALS, beta-band (15–30 Hz) intermuscular coherence was explored by [28] and latter by [29] to determine whether it can distinguish ALS patients from normal subjects. The authors of [29] collected a dataset with 15 ALS and 15 control subjects and achieved a sensitivity of 87% and specificity of 87%. The authors of [30] propose an automated machine learning pipeline with features extracted from sEMG using *tsfresh* [31]. They used a dataset composed of 65 subjects (20 with the inclusion of body myositis, 20 with ALS and 25 healthy control). Two classification strategies were designed: muscle-level, meaning the prediction is accomplished for each muscle of all subjects individually; patient-level, which relied on classification voting ensembles on the muscles from the same patient. They classified each subject as being either patient or healthy and achieved an Area Under the Curve (AUC) score of 81.7% and 81.5% for muscle-level and patient-level, respectively. The authors of [32] used a set of statistical, temporal, complexity, and fractal features from sEMG recordings in the limbs. They used a dataset composed of 33 subjects (13 with ALS and 20 healthy control). The authors tested several machine learning classifiers, where the decision tree, random forest, and AdaBoost, achieved the highest performance. An average accuracy of 77% was achieved by combining differences between features extracted from the hand and forearm recordings. More recently, the authors of [33] attained accurate classification performance on a dataset composed of 13 patients with ALS and 10 healthy controls with electrodes configured for facial sEMG collection.

Further works using nEMG or sEMG in the context of ALS diagnosis, can be followed in [34], which recently conducted a systematic literature review on machine learning techniques and biomedical signals in the context of ALS. The number of works using nEMG has been higher compared to sEMG, which motivates the need for more contributions in the context of sEMG.

The clinical interpretation of a nEMG exam relies on the analysis of MUAP waveforms. Quantitative measurements are conducted by the clinician, such as MUAP amplitude, duration, number of phases, firing rate, among others [35]. The quantitative measurements calculated using feature extraction from the studies identified above do not place a strong emphasis on the MUAPs morphology. Quite often, prior studies use a set of statistical, temporal, and spectral features to evaluate the EMG into a more high-level setting. Nevertheless, changes in the shape of surface representations of MUAPs measured by sEMG are helpful to identify possible pathological changes in MU activity patterns [36]. Therefore, there is a gap in the literature regarding using morphological features for MUAPs, which can later be used for ML algorithms. These features would be representative of the morphology of the MUAPs based on their surface sEMG representations. Furthermore, they could more objectively depict the changes in the EMG caused by ALS: reinnervation potentials, which result in higher amplitude MUAPs; loss of MUs, translating into an increased firing rate of the active MUs; and evidence of FPs, marked by abrupt spikes [9].

The use of morphological features to complement the feature sets which are typically used would present some advantages. Those features might capture complementary discriminate behaviors on the waveform as the disease progresses. Additionally, since those features are inspired by clinical interpretation, they can lead to more interpretable predictions from the classifiers. These features would include the detection of MUAPs of a sEMG signal, which is the process of identifying and isolating the surface representations of MUAPs. Since the measured muscle has a limited number of MUs, each originating a unique MUAP, the signal can be decomposed into the different firing MUAPs. This process starts with the detection of MUAPs, followed by their categorization into one of the originating MUs.

In this paper, we propose a novel set of morphological features for EMG analysis. Our contributions are focused on the introduction

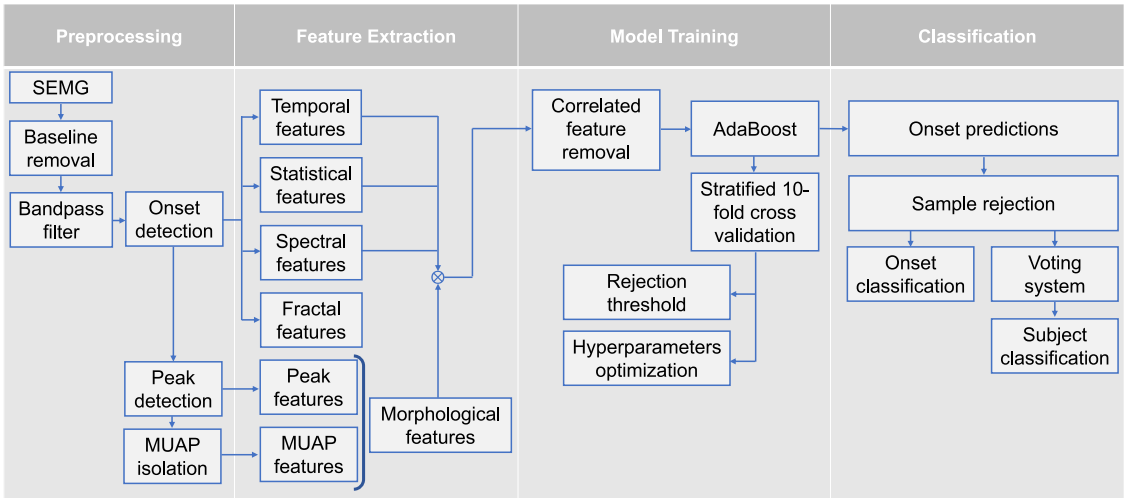

Fig. 2. Schematic representation of the proposed machine learning pipeline.

of a signal processing pipeline to compute the morphological features on sEMG and a validation study for automated ALS diagnosis using a cohort of control and ALS patients. The proposed features were included as an add-on to the open-source Python library entitled Time Series Feature Extraction Library (TSFEL) [37].

The rest of this paper is organized as follows: Section 2 presents the proposed set of morphological features, describes the dataset and the proposed machine learning pipeline. The results are presented in Section 3 and discussed in Section 4. Finally, Section 5 summarizes the contributions and limitations of this work, along with some recommendations for future work.

2. Materials and methods

We implemented a ML pipeline to validate the proposed sEMG features in a binary classification task, as represented in Fig. 2. The goal of this task was to distinguish between pathological and healthy sEMG signals. The first stage addresses the preprocessing steps, particularly signal filtering and window segmentation of muscular activation intervals. Secondly, several features are extracted and combined into the final feature vector that describes each window. Next, the features are used for the learning stages, hyperparameter optimization, and feature selection. Lastly, the learning stage is repeated with the optimized hyperparameters and selected features, and the final classification task is performed.

This section also encloses the description of the experimental protocol in which data were collected.

2.1. Data

We used an anonymized dataset that we collected and previously explored in [38], where a more detailed description of the experimental protocol can be found. The data was acquired from two different subsets of subjects: healthy controls (HCs) and patients diagnosed with ALS within the preceding 36 months, with a muscle strength greater than three according to the Medical Research Council scale (MRC scale), in the tested muscles. Patients could not present any other neurological disorders. All patients were medicated with Riluzole [39].

The ALS patient population was initially comprised of 21 subjects. The patients were divided into two categories depending on their disease phenotype. Since bulbar-onset patients do not often express significant abnormalities with sEMG recordings at the upper arms, the spinal-onset patients were the only ones considered for further analysis, resulting in 17 subjects, seven men and ten women, with a mean age of 59 ± 10. A group of 24 healthy subjects was considered, nine men and 15 women. Therefore, the final dataset totaled 41 subjects, 17 diagnosed with the spinal onset of ALS and 24 HCs.

The study was performed in accordance with the ethical standards of the 1964 Helsinki Declaration and its later amendments. Ethical approval for this research was obtained from the Ethics Committee of Centro Hospitalar Universitário Lisboa Norte. Informed consent was obtained from all individual participants involved in the study.

Fig. 3 shows the experimental setup. Subjects were seated with both hands and forearms on a desk in a parallel position, 10 cm away from each other with hand palms facing one another in 90 degrees flexion with the elbow. Then, they were asked to perform the same movement on both left and right hands while listening to a programmed sound, which guided the task. This task was a coordinated movement of vertical elevation of both index fingers in the opposing direction of the remaining fingers, reaching maximum articular amplitude. The subject would then hold that position with a certain degree of force for three seconds, return to the original position and remain in that position for three seconds while trying to relax as much as possible. The task was repeated for six minutes or less, depending on the maximum time tolerated by the patients. Each muscle had two surface electrodes connected. The electrodes were fixed on the first dorsal interosseus muscle for both hands, with the reference electrode on the first interphalangeal joint of the index finger, and the *extensor digitorum communis* muscle for both forearms, with the reference electrode 3 cm distal. The ground was placed on ulna bone inferior extremity since no muscle activity is present in that region. The electrode placement protocol resulted in the recording of four time-synchronized signals for each subject [38].

All recordings were performed with a biosignalsplux (Plux, Lisbon, Portugal) biomedical data collection system with eight analog input channels converted to 12-bit signals and an external channel used as reference ground. The sEMG sensors include 2nd order bandpass analog filters with 25 and 450 Hz cut-off frequencies adjacent to the electrodes. The sEMG signals were acquired with a gain of 1000 and a sampling frequency of 1000 Hz.

The first channel refers to the left hand, the second channel refers to the left forearm, and the third channel refers to the right hand. The fourth channel was discarded since no complete data were available for all subjects.

2.2. Preprocessing

The first step of the preprocessing consisted of filtering the recordings by removing the baseline offset and then applying a 3rd order Butterworth bandpass filter between the frequencies of 10 and 300 Hz. Since we were interested in analyzing the intervals where the subject

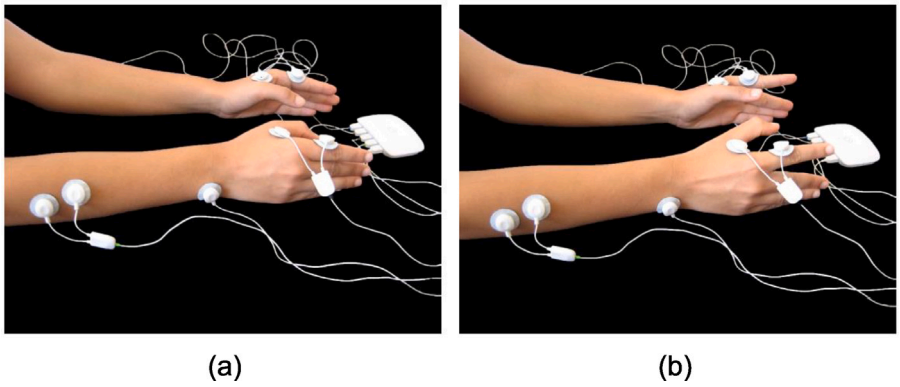

Fig. 3. Experimental setup. The electrodes were attached on the first dorsal interosseus muscle for both hands and the *extensor digitorum communis* muscle for both forearms. The ground electrode was attached to the ulna bone inferior extremity. The signals were recorded using a biosignalsplux biomedical data collection system. The subjects were asked to perform consecutive repetitions between resting and contraction periods [38].

performed muscular contractions, an onset detector based on Teager–Kaiser Energy Operator (TKEO) was applied [40]. Afterward, a careful visual inspection was conducted on each record to ensure that the onset detection result was in accordance with the muscular contraction intervals. A total of 3592 contractions was detected for the 41 subjects, of which 54% were healthy samples and 46% pathological samples. It is important to mention that there was some variability in the number of contractions among the subjects, with an average number of onsets of 88 ± 16 per acquisition.

2.3. Feature extraction

After the preprocessing and muscular contraction detection, we extracted several features for each contraction interval. Therefore, each contraction period was represented into a k-dimensional real-valued feature vector, where k is the total number of features. The resting intervals between muscular contractions were not considered. The features were extracted from the three available channels.

We explored a wide variety of features to characterize the recordings. A set of state-of-the-art EMG features was combined with the proposed set of features to understand their discriminating value in sEMG for ALS diagnosis. We used the TSFEL open-source library [37] to extract time-, statistical-, and spectral-domain features with default settings. Based on the work from [38] fractal-domain features were also extracted. Finally, the proposed group of peak-related and MUAP morphology features were considered. This totals 196 features. These features were extracted for the three channels, resulting in 588 features. The computation of the pairwise correlation of features using the Pearson correlation method excluded the features whose correlation was higher than 0.95. Thus a total of 317 features per muscular activation interval was considered.

A list of all the features considered is available in Appendix.

2.3.1. Novel features

We propose two groups of novel features: peak-related and MUAP morphology features. A brief description of these 18 new features can be found in Table 1. The first group quantifies statistical characteristics related to the positive peaks of the signal. The second one provides quantitative measurements related to the MUAP morphology, which are summarized in Fig. 4. These features were designed under the hypothesis that they can be more interpretable, as they measure morphological characteristics that represent physiological processes that are taken into account in clinical interpretation to diagnose neuropathies.

The signal processing pipeline designed to obtain the novel features includes detecting the signal's peaks and isolating the surface representations of individual MUAPs. The MUs activated during muscular contraction generate MUAPs and their summation yields the sEMG signal. The sEMG decomposition consists of segmenting and identifying the constituent MUAPs. Our approach for MUAP isolation consists of (1) identifying all the significant local maxima during muscle activation periods and (2) post-process the detected peaks to isolate the MUAP waveform in their neighborhood. An overview of the processing workflow is depicted in Fig. 5.

Table 1
Description of the proposed peak-related and morphology features.

Feature	Description
Peak-related features	
Number of peaks	Total number of peaks
Peaks difference	Time interval between consecutive peaks
Peaks rate	Number of peaks per second
MUAP morphology features	
Peak-to-peak amplitude	Amplitude from the lowest negative peak to the highest positive peak of the MUAP
Peak-to-peak difference	Time interval between the lowest negative peak to the highest positive peak of the MUAP
MUAP duration	Time interval during which the MUAP occurs
MUAP integrated area	Absolute area of the MUAP
MUAP rise time	Time interval between maximum negative peak and the following minimum positive peak within the duration of the MUAP
MUAP phases	Number of baseline crossings within the duration where amplitude exceeds the mean of the signal
MUAP turns	Number of positive and negative peaks where the differences from the preceding and following turn exceed 25 μV

Firstly, a local maximum is considered significant if its amplitude is higher than the 98-th percentile of the muscular onset interval and the distance between consecutive maxima has a minimum value of 20 ms, to prevent the detection of peaks related to noise. Using the peaks obtained in this step, the peak-related features were extracted for each muscular contraction window of the signal. The number of peaks and peaks rate were directly quantified. The peaks difference was determined for each pair of consecutive peaks and then averaged, resulting in two features which were the average and standard deviation of this measure.

The detected peaks and the waveform are then processed according to Algorithm 1. We provide below a thoroughly description of the algorithm.

We considered an interval before and after the peak, p, to delimit the MUAPs around the previously detected peaks. The window size, w, was set to 20 ms centered in each detected peak, as the average MUAP duration ranges from 10 ms to approximately 30 ms [41].

Next, we found the positions and amplitudes of the global maxima and minima of the considered window to measure the peak-to-peak

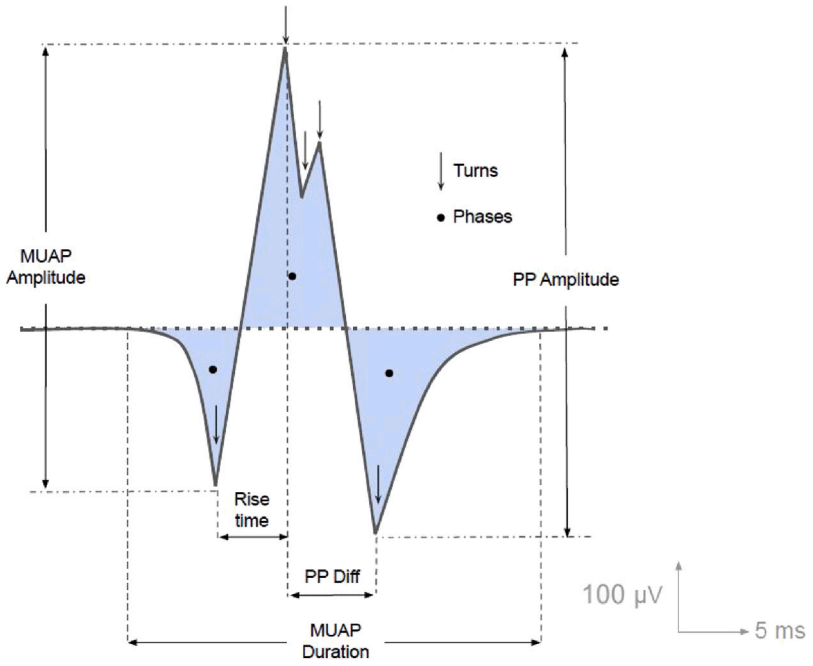

Fig. 4. Quantitative characteristics of MUAP waveforms. "PP" corresponds to peak-to-peak.

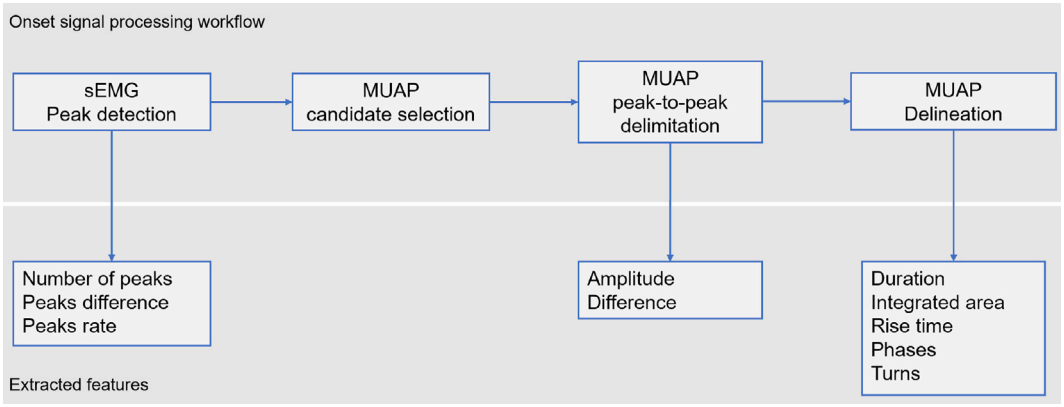

Fig. 5. Schematic representation of the proposed MUAP isolation pipeline.

distance and peak-to-peak time interval. These peak-to-peak measures were determined for each MUAP within the muscular contraction onset, and then their mean and respective standard deviation were calculated, resulting in a total of four features.

To calculate the remaining morphology features, the MUAP waveform was isolated through the detection of plateaus around the main peak. We extended the candidate interval with a neighborhood of 1 ms before and after the positions of the previously mentioned global maxima and minima. A threshold (Δ) was defined as a fraction of the peak-to-peak amplitude calculated along with this candidate interval. A neighborhood search procedure before and after the candidate interval was conducted to find the positions where the signal amplitude exceeds Δ. The first samples greater than Δ are the MUAP start and ending positions. This last processing stage allowed the extraction of the remaining ten features, namely the MUAP duration, integrated area, rise time, phases, and turns. Similar to the procedure adopted for peak-to-peak measures, the measures were determined first for each MUAP within a muscular contraction interval, and then we considered the average and standard deviation of the respective measures.

2.4. Classification

A supervised classification approach was applied to discriminate between subjects with ALS and HCs. The selected model was an AdaBoost classifier, using Random Forest as the base estimator. The learning phase started with the optimization of the model by iteratively experimenting with different groups of the model's hyperparameters in the classification task. All available features from the train data were considered for this task, throughout ten folds of Shuffle-Group-Out Cross-Validation [42]. The most common group of hyperparameters maximizing the F_1 score metric throughout all folds was selected as the ideal set of hyperparameters. Then, the model was retrained with the optimized hyperparameters and multiple train samples as input, guaranteeing that all samples from each subject were either on the training set or on the test set. Since one subject has multiple activation intervals, each interval with a set of features extracted, each sample was classified separately.

To improve the robustness of the proposed method, class probabilities were used for sample rejection, which eliminated signal windows whose attributed class had a probability value lower than an optimal threshold. The rejected windows were not considered for the overall classification performance. According to a method proposed by [43],

Algorithm 1: MUAP isolation algorithm.

FIND_MAJOR_PEAKS returns the positions of the global maxima and minima of a given signal. PEAKTOPEAK calculates the peak-to-peak amplitude of a given signal.

Input:
- $OnsetWaveForm$ ▷ An array with SEMG data for a given onset interval.
- $peaks$ ▷ The array positions of the MUAP's peaks.
- w ▷ MUAP maximum duration interval (s)
- f_s ▷ Sampling frequency (Hz).
- δ ▷ Fraction of the peak-to-peak amplitude to consider.

Output:
- $StartEndPosPairs$ ▷ A list of start and end position pairs for each MUAP.

$StartEndPosPairs = [\ ]$
for p in $peaks$ **do**
  $CandidateWindowedWaveform \leftarrow OnsetWaveform[p - \frac{w \times f_s}{2} : p + \frac{w \times f_s}{2}]$
  $MuapMajorPeaks \leftarrow$ FIND_MAJOR_PEAKS($CandidateWindowedWaveform$)
  $StartPos = MuapMajorPeaks[0] - (1 \times f_s)$
  $EndPos = MuapMajorPeaks[1] + (1 \times f_s)$
  $\Delta \leftarrow$ PEAKTOPEAK ($CandidateWindowedWaveform[StartPos : EndPos]$) $\times\ \delta$

  Do a neighborhood search of $\frac{w \times f_s}{2}$ samples before $StartPos$
  if any sample in neighborhood $>= \Delta$ **then**:
    $MuapInitPos \leftarrow SamplePos$ ▷ $SamplePos$ is the first sample found.
  else
    $MuapInitPos \leftarrow p - \frac{w \times f_s}{2}$
  end if

  Do a neighborhood search of $\frac{w \times f_s}{2}$ samples after $EndPos$
  if any sample in neighborhood $>= \Delta$ **then**:
    $MuapEndPos \leftarrow SamplePos$ ▷ $SamplePos$ is the first sample found.
  else
    $MuapEndPos \leftarrow p + \frac{w \times f_s}{2}$
  end if

  $StartEndPosPairs \leftarrow [MuapInitPos, MuapEndPos]$
end for
return $StartEndPosPairs$

the optimal threshold θ_{opt} for rejection cost b was obtained using the following equation:

$$\theta_{opt}(b) = arg\max_{\theta} \left(|\mathcal{E}_\theta| - \frac{b}{1-b} \cdot |\mathcal{L}_\theta| \right) \quad (1)$$

where θ is a probability threshold in the interval $[0, 1]$, $\mathcal{E}_\theta$ and $\mathcal{L}_\theta$ represent the subset of true rejects and false rejects for the threshold θ, respectively. The rejection cost value b was set to 0.5.

A voting system that took into account all samples from one signal was implemented to provide a diagnosis for the subject. This diagnostic criterion counts the number of healthy classified samples as the number of votes for the HC class, and the corresponding samples for the ALS class. The class with the most votes was considered the final decision of the classifier for that signal. Therefore, two different types of classification tasks were performed: **onset classification** and **subject classification**. The latter consists of implementing the voting system that considers the information given by the onset classification task.

A 10-fold Shuffle-Group-Out Cross-Validation scheme that split the number of subjects in half for train and test sets in each fold was used. The group of chosen subjects for train and test in a fold was the same throughout all experiments in that specific fold so that outcomes from different experiments could be compared.

3. Results

This section presents the results of the onset and subject classification approaches. It reports the average results of the Cross-Validation scheme.

The accuracy, precision, recall, and F_1 score were used to assess the classification performance. Accuracy is the overall probability of correctly classified instances over the total number of instances. Precision is the ratio between correctly classified ALS instances and the total number of instances classified as ALS. The recall is the ratio between correctly classified ALS instances and the total number of ALS instances. F_1 score is the harmonic mean of precision and recall. Except for accuracy, all metrics were macro-averaged since the dataset was approximately balanced in terms of pathological and healthy samples, giving a more generalized performance measure irrespective of the class. However, the subject classification task presented a slight imbalance since the dataset contained a higher number of healthy subjects.

Table 2
Onset classification results obtained by using each feature group separately measured by means of F_1, precision, recall, and accuracy scores. The scores are presented in percentage (%) as the average of ten folds with the respective standard deviation. The best scores per metric are highlighted in bold.

	F_1 score	Precision	Recall	Accuracy
Temporal	68.9 ± 7.8	77.0 ± 4.5	69.3 ± 5.7	73.4 ± 6.1
Spectral	**81.2 ± 4.7**	**85.3 ± 3.7**	**80.7 ± 4.2**	**82.8 ± 4.6**
Statistical	69.2 ± 8.6	74.6 ± 6.4	70.0 ± 6.9	73.0 ± 7.9
Fractal	71.5 ± 9.9	78.7 ± 4.1	72.3 ± 7.3	75.5 ± 6.9
Proposed	77.1 ± 3.2	80.7 ± 4.0	76.7 ± 2.7	78.9 ± 3.4

Table 3
Subject classification results obtained by using each feature group separately measured by means of F_1, precision, recall, and accuracy scores. The scores are presented in percentage (%) as the average of ten folds with the respective standard deviation. The best scores per metric are highlighted in bold.

	F_1 score	Precision	Recall	Accuracy
Temporal	67.3 ± 10.1	74.1 ± 10.0	68.7 ± 7.3	70.0 ± 9.5
Spectral	**75.4 ± 7.8**	**79.5 ± 7.6**	**76.1 ± 7.3**	**76.7 ± 7.5**
Statistical	69.6 ± 8.4	74.6 ± 7.9	70.7 ± 7.5	71.4 ± 8.3
Fractal	69.7 ± 10.6	77.2 ± 5.9	71.5 ± 7.9	72.4 ± 9.0
Proposed	70.8 ± 4.7	75.5 ± 6.1	71.9 ± 4.1	72.4 ± 4.7

The onset and subject classification results, which will be presented below, are not comparable, considering they represent distinct outcomes of the same signal. We conducted several experiments to evaluate the proposed pipeline in the onset and subject classification approaches.

The first experiment consisted of training the model with the five feature sets separately, to evaluate the individual predictive capability of each set. Table 2 summarizes the performance scores for the onset classification approach using each feature set individually. The spectral features produced the overall best results, followed by the set of proposed features. On the other hand, the temporal and statistical groups performed relatively poorly, with overall lower scores.

Table 3 summarizes the performance scores for the subject classification approach using each set feature set individually. The results are in agreement with the outcome for the onset classification task, with the group of features with the best overall scores being the spectral, followed by the proposed feature set.

In the second experiment, we evaluated how the individual introduction of the proposed feature set would impact the classification. We hypothesized that introducing the proposed feature set to the feature group containing all the remaining features (i.e., temporal, statistical, spectral, and fractal) would increase the overall classification results.

Table 4 shows a comparison of the onset classification performance when using the temporal, spectral, statistical, and fractal features and when considering all features by introducing the proposed feature sets. The results support the hypothesis that combining the proposed feature set with the remaining features would increase the overall performance. This hypothesis was further validated in the subject classification approaches, whose results are presented in Table 5.

In the previous experiments, we considered the available data from the three channels. In order to reduce the complexity for both data collection and processing in real ambulatory settings, a single-channel configuration would be desirable. In the third experiment, we evaluated the classification performance of each channel individually.

Table 4
Onset classification results obtained by using all feature groups and all features except the proposed ones, measured by means of F_1, precision, recall, and accuracy scores. The scores are presented in percentage (%) as the average of ten folds with the respective standard deviation. The best scores per metric are highlighted in bold.

Feature set	F_1 score	Precision	Recall	Accuracy
Temporal Spectral Statistical Fractal	80.0 ± 3.0	85.2 ± 1.9	79.0 ± 3.0	82.6 ± 3.3
All	**83.1 ± 4.2**	**86.9 ± 2.8**	**82.1 ± 4.2**	**84.8 ± 3.7**

Table 5
Subject classification results obtained by using all feature groups and all features except the proposed ones by means of F_1, precision, recall, and accuracy scores. The scores are presented in percentage (%) as the average of ten folds with the respective standard deviation. The best scores per metric are highlighted in bold.

Feature set	F_1 Score	Precision	Recall	Accuracy
Temporal Spectral Statistical Fractal	76.6 ± 5.8	81.2 ± 6.0	76.9 ± 5.4	78.1 ± 5.7
All	**78.9 ± 6.0**	**82.3 ± 6.0**	**78.8 ± 5.3**	**80.00 ± 6.0**

Table 6
Onset classification results obtained by using all features from each channel and from all channels simultaneously, measured by means of F_1, precision, recall, and accuracy scores. The scores are presented in percentage (%) as the average of ten folds with the respective standard deviation. The best scores per metric are highlighted in bold.

	F_1 score	Precision	Recall	Accuracy
Left hand	68.9 ± 5.7	76.0 ± 3.7	70.4 ± 5.6	71.9 ± 4.4
Left forearm	72.3 ± 7.9	79.7 ± 9.0	71.7 ± 6.9	76.1 ± 8.2
Right hand	81.9 ± 5.1	84.9 ± 5.5	81.3 ± 4.9	83.0 ± 5.3
All channels	**83.1 ± 4.2**	**86.9 ± 2.8**	**82.1 ± 4.2**	**84.8 ± 3.7**

Table 7
Subject classification results obtained by using all features from each channel and from all channels simultaneously, measured by means of F_1, precision, recall, and accuracy scores. The scores are presented in percentage (%) as the average of ten folds with the respective standard deviation. The best scores per metric are highlighted in bold.

	F_1 score	Precision	Recall	Accuracy
Left hand	65.5 ± 10.5	71.9 ± 9.7	67.8 ± 9.4	68.1 ± 9.3
Left forearm	66.8 ± 10.8	76.1 ± 12.0	68.5 ± 9.9	69.5 ± 10.5
Right hand	**79.4 ± 8.4**	**83.7 ± 7.9**	**79.4 ± 7.8**	**80.9 ± 7.9**
All channels	78.9 ± 6.0	82.3 ± 6.0	78.8 ± 5.3	80.0 ± 6.0

Table 6 summarizes the results for the onset classification approach in using individual channels and considering all the available channels. The best results for the onset classification approach were achieved when considering all three channels. For the subject classification task, the best results were achieved for the right first dorsal interosseous muscle, as shown in Table 7. Therefore, the right first dorsal interosseous muscle showed interesting results with competitive performance results in a single-channel configuration. Using a single channel setup reduces the number of features by two-thirds, increasing the computational processing speed, which is crucial when performing feature selection.

The results suggest that the right first dorsal interosseous muscle yields reasonable diagnosis performance alone. For this reason, it was further explored in the additional experiments.

In the next experiment, we explored the classification performance for each feature set considering only the right first dorsal interosseous muscle. The results are presented in Tables 8 and 9. In both classification approaches, the proposed feature set achieved the highest performance values compared to the other individual feature sets. These results suggest that the proposed feature set can diagnose ALS muscular contraction intervals with a reasonable performance. In comparison with previous experiments, the performance values were achieved using a single-channel configuration and a single feature set.

Table 8
Onset classification results obtained by using each feature group separately extracted from the right first dorsal interosseus only, measured by means of F_1, precision, recall, and accuracy scores. The scores are presented in percentage (%) as the average of ten folds with the respective standard deviation. The best scores per metric are highlighted in bold.

	F_1 score	Precision	Recall	Accuracy
Temporal	73.2 ± 6.3	79.3 ± 5.6	73.1 ± 6.0	76.9 ± 4.7
Spectral	78.6 ± 4.8	81.5 ± 5.2	78.4 ± 4.8	79.7 ± 4.8
Statistical	76.5 ± 4.1	80.0 ± 3.7	76.7 ± 3.7	77.9 ± 3.9
Fractal	77.4 ± 7.1	80.9 ± 6.3	77.1 ± 7.2	79.6 ± 6.2
Proposed	**81.9 ± 5.7**	**84.0 ± 4.9**	**81.9 ± 5.5**	**82.6 ± 5.6**

Table 9
Subject classification results obtained by using each feature group separately extracted from the right first dorsal interosseus only, measured by means of F_1, precision, recall, and accuracy scores. The scores are presented in percentage (%) as the average of ten folds with the respective standard deviation. The best scores per metric are highlighted in bold.

	F_1 score	Precision	Recall	Accuracy
Temporal	74.3 ± 6.5	81.5 ± 5.3	75.2 ± 4.7	76.2 ± 6.4
Spectral	76.0 ± 5.9	81.1 ± 6.7	76.3 ± 5.4	77.6 ± 5.7
Statistical	77.6 ± 4.9	80.2 ± 5.4	77.9 ± 5.2	78.6 ± 4.9
Fractal	78.8 ± 9.4	83.1 ± 8.6	79.3 ± 8.6	80.0 ± 9.0
Proposed	**83.6 ± 6.9**	**86.6 ± 6.5**	**83.7 ± 6.3**	**84.3 ± 6.8**

4. Discussion

Prior work on the development of machine learning approaches for automated ALS diagnosis using sEMG often relies on temporal, frequency, and time–frequency feature sets. The use of a morphological feature set based on the MUAP characterization to complement existing features sets can lead to more interpretable predictions from classifiers since the design of the morphological feature set would be inspired by the clinical interpretation of the EMG trace.

Two classification approaches were considered, whose results are independent and incomparable, since the voting system used for the patient classification attributes the same class to all the contraction intervals of each patient, which may not correspond to the truth.

The results suggest that the proposed data collection and processing setup is feasible to diagnose ALS. The best result for the onset classification approach, with an F_1 score of 83.1 ± 4.2%, was achieved using a comprehensive group of features extracted from three channels. The rejection rate was 27%. The rejection rates during the onset classification experiments achieved slightly high values. However, it is quite challenging to issue a diagnosis based on a single onset with high certainty. These rejection rates did not affect the performance of the subject classification approach since they relied on information about multiple onset intervals and, thus, the classifier did not reject any subjects. With further experiments, we also identified that using a single channel on the right first dorsal interosseous muscle and only relying upon the proposed set of features, an F_1 score of 82.0 ± 5.7% was achieved. Although by a slight difference, the classifier precision was higher than recall.

The best result for the patient classification approach was achieved when using the proposed feature set from the right first dorsal interosseous muscle, with an F_1 score of 83.6 ± 6.9%.

Our experiments showed that using only the right hand it is possible to achieve competitive performance in comparison to combining channels from both upper limbs. These results are in line with previous experiments that support evidence that when the region of the upper limbs is the region of disease onset, the right arm is frequently first affected than the left arm [44].

Achieving high classification performance with lower data collection and processing complexity has both analytical and practical implications. Model performance might degrade when including features not relevant to the target variable. Additionally, a large number of features

can slow the training and development of models and require higher computational performance. From the application standpoint, using a single channel and a reduced yet efficient feature set is important, particularly for remote examination in patients' homes.

Our classification results are in accordance with previously published works on diagnosis using machine learning approaches with sEMG [32,45]. The dataset used in our work was collected by Quintão et al. [32], which reported an average accuracy of 77% when classifying between ALS patients and controls. In the present work, we achieved a higher average accuracy value of 84.8 ± 3.7 considering all channels and feature sets and 82.6 ± 5.6 as the best single-channel using only the proposed features. However, one should mention that the authors of [32] considered different classification models, multiple channel combinations, and several feature sets.

The empirical results reported herein should be considered in light of some limitations. The proposed feature set, based on peak and morphology-related features, relies on the assumption of correct identification of MUAPs in the recording. The sEMG decomposition into MUAPs is per se a challenging topic in EMG signal processing and often relies on highly complex approaches for the data collection protocol and data processing techniques [11,46]. Over the last years, there have been several proposed approaches for EMG decomposition [47,48], which are complex and still have some shortcomings. We opted for a simple approach that allowed a significant amount of surface MUAPs to be considered. Although our proposed method might come short compared to more sophisticated alternative methods, we argue that it can still be applied for a preliminary assessment between control and ALS groups using our proposed set of features. This approach does not ensure that all detected peaks are actually representative of a MUAP, and it does not take into account that MUAP duration presents a high degree of variability [49]. Nevertheless, we argue that it can still extract relevant quantitative information from the morphology of the surface potentials of the MUAPs contained in the recordings. Visual inspection of the results showed good qualitative results, although it also revealed some false positives and false negatives arising from noise and MUAPs superimpositions. The fact our approach does not need highly complex data collection protocols and processing techniques, make it an interesting method to be applied in remote ambulatory settings.

5. Conclusions

The non-invasive nature of the sEMG offers significant practical advantages over invasive methods, such as the possibility to monitor the disease with less discomfort for the patient. Although in the past there has been some discredit in the medical community regarding the lack of evidence to determine the clinical utility of sEMG, recent technological advances have reignited the awareness of the community for this versatile technique. Therefore, there is currently the need for multi-disciplinary collaboration to tackle the remaining analytical and technical challenges of sEMG [13].

In this work, we proposed a novel feature set for the characterization of sEMG based on the quantification of morphological properties of surface potentials from MUs. Our contributions were the introduction of a signal processing pipeline to compute such features and a machine learning pipeline for automated ALS diagnosis. Our methods were validated using a dataset with a cohort of control and ALS patients with sEMG recordings of the upper limbs.

The present research contained several experiments which showed promising results that uncovered the benefits of introducing morphological information into automated diagnosis machine learning pipelines. The recordings from the right first dorsal interosseous muscle revealed particularly interesting results. Minimizing the complexity of the data collection setup using a single muscle and a reduced feature set has several practical benefits. A more convenient data collection setup helps pave the way for remote examination at patients' residences, increasing the data available for clinicians towards better diagnosis, prognosis, and shared decision-making on ALS.

Previous studies relied on conventional temporal, statistical, and spectral-domain feature sets. Our proposed morphological feature set has proved competitive classification performance and can lead to more interpretable predictions from the classifier since the design of such features was inspired by the clinical interpretation of EMG data. It is worth mentioning that the morphological feature set relies on a prior decomposition of the sEMG to identify the surface potentials generated by MUs. The decomposition of sEMG is non-trivial, and despite relying on a simple approach, identified as a current shortcoming, the results were still promising. Our work also aims to spark future research on automated analysis methods to exploit the practical utility of sEMG. The proposed features were included as an add-on to TSFEL.

In future work, we will improve the method used for sEMG decomposition. Since the results showed the feasibility of our approach, we will research the integration of explainable artificial intelligence methods to measure the feature relevance and explain the classifier predictions. It is expected that the proposed feature set should help design transparent and trustworthy automated decision support systems. Furthermore, it would be interesting to conduct a longitudinal evaluation study in the context of ALS prognosis.

Table A.1
Description of the feature sets.

Domain	Features
Time	Absolute energy
	Absolute value of summation of exponential root
	Absolute value of summation of square root
	Area under the curve
	Autocorrelation
	Autoregressive coefficients
	Average amplitude change
	Cardinality
	Centroid
	Difference absolute mean value
	Difference absolute standard deviation value
	Difference variance value
	Enhanced wavelength
	Entropy
	Integrated EMG
	Log detector
	Log difference absolute standard deviation
	Log difference absolute mean value
	Log Teager Kaiser energy operator
	Mean absolute difference
	Mean difference
	Mean absolute value slope
	Mean value of square root
	Median absolute difference
	Median difference
	Myopulse percentage rate
	Negative turning points
	New zero crossing
	Neighborhood peaks
	Peak to peak distance
	Positive turning points
	Signal distance
	Slope
	Slope sign change
	Sum absolute difference
Time	Temporal moment
	Total energy
	V-Order
	Waveform length
	Willison amplitude
	Zero crossing rate

(*continued on next page*)

Table A.1 (*continued*).

Domain	Features
Spectral	Fundamental frequency
	Human range energy
	Linear prediction cepstral coefficients
	Mel-frequency cepstral coefficients
	Maximum power spectrum
	Maximum frequency
	Median frequency
	Power bandwidth
	Spectral centroid
	Spectral decrease
	Spectral distance
	Spectral entropy
	Spectral kurtosis
	Spectral positive turning points
	Spectral roll-off
	Spectral roll-on
	Spectral skewness
	Spectral slope
	Spectral spread
	Spectral variation
	Wavelet absolute mean
	Wavelet energy
	Wavelet entropy
	Wavelet standard deviation
	Wavelet variance
Statistical	Average energy
	Values of the empirical cumulative distribution function (ECDF)
	ECDF percentile
	Coefficient of variation
	ECDF percentile count
	ECDF slope
	Enhanced mean absolute value
	Histogram
	Interquartile range
	Kurtosis
	Log coefficient of variation
	Maximum
	Mean
	Mean absolute deviation
	Mean absolute value
	Median
	Median absolute deviation
	Minimum
	Modified mean absolute value type 1
	Modified mean absolute value type 2
	Root mean square
	Skewness
	Standard deviation
	Variance
Fractal	Fractal Dimension
	Maximum Fractal Length
	Multiscale entropy
	Lempel–Ziv Complexity
	Detrended Fluctuation Analysis

CRediT authorship contribution statement

Margarida Antunes: Conceptualization, Methodology, Software, Investigation, Writing – original draft. **Duarte Folgado:** Conceptualization, Methodology, Investigation, Writing – original draft. **Marília Barandas:** Writing – review & editing. **André Carreiro:** Writing – review & editing. **Carla Quintão:** Validation, Data curation, Writing – review & editing. **Mamede de Carvalho:** Writing – review & editing. **Hugo Gamboa:** Writing – review & editing, Supervision.

Declaration of competing interest

The authors declare that they have no known competing financial interests or personal relationships that could have appeared to influence the work reported in this paper.

Acknowledgments

This work was supported by national funds from FCT Foundation for Science and Technology, Portugal, I.P. through the protect HomeSenseALS: Home-based monitoring of functional disability in amyotrophic lateral sclerosis with mobile sensing with reference PTDC/MEC-NEU/6855/
2020 and research unit UIDB/FIS/04559/2020 (LIBPhys-UNL).

Appendix. Description of the feature sets

See Table A.1.

References

[1] R.S. Snell, Clinical Neuroanatomy, seventh ed., Lippincott Williams & Wilkins, 2010.
[2] L.I. Grad, G.A. Rouleau, J. Ravits, N.R. Cashman, Clinical spectrum of amyotrophic lateral sclerosis (ALS), Cold Spring Harb. Perspect. Med. 7 (8) (2017) a024117, http://dx.doi.org/10.1101/cshperspect.a024117.
[3] E. Longinetti, F. Fang, Epidemiology of amyotrophic lateral sclerosis, Curr. Opin. Neurol. 32 (5) (2019) 771–776, http://dx.doi.org/10.1097/WCO.0000000000000730.
[4] R.B. Daroff, M.J. Aminoff, Encyclopedia of the Neurological Sciences, second ed., Elsevier Science, Academic Press, 2014.
[5] E. Tiryaki, H.A. Horak, ALS and other motor neuron diseases, Contin. Lifelong Learn. Neurol. 20 (5) (2014) 1185–1207, http://dx.doi.org/10.1212/01.CON.0000455886.14298.a4.
[6] J. Duchateau, R.M. Enoka, Human motor unit recordings: Origins and insight into the integrated motor system, Brain Res. 1409 (2011) 42–61, http://dx.doi.org/10.1016/j.brainres.2011.06.011.
[7] C.K. Thompson, F. Negro, M.D. Johnson, M.R. Holmes, L.M. McPherson, R.K. Powers, D. Farina, C.J. Heckman, Robust and accurate decoding of motoneuron behaviour and prediction of the resulting force output, J. Physiol. 596 (14) (2018) 2643–2659, http://dx.doi.org/10.1113/JP276153.
[8] B.R. Brooks, R.G. Miller, M. Swash, T.L. Munsat, El escorial revisited: Revised criteria for the diagnosis of amyotrophic lateral sclerosis, Amyotroph. Lateral Scler. Other Mot. Neuron Disord. 1 (5) (2000) 293–299, http://dx.doi.org/10.1080/146608200300079536.
[9] M. de Carvalho, R. Dengler, A. Eisen, J.D. England, R. Kaji, J. Kimura, K. Mills, H. Mitsumoto, H. Nodera, J. Shefner, M. Swash, Electrodiagnostic criteria for diagnosis of ALS, Clin. Neurophysiol. 119 (3) (2008) 497–503, http://dx.doi.org/10.1016/j.clinph.2007.09.143.
[10] X. Zhang, P.E. Barkhaus, W.Z. Rymer, P. Zhou, Machine learning for supporting diagnosis of amyotrophic lateral sclerosis using surface electromyogram, IEEE Trans. Neural Syst. Rehabil. Eng. 22 (1) (2014) 96–103, http://dx.doi.org/10.1109/TNSRE.2013.2274658.
[11] D. Farina, F. Negro, M. Gazzoni, R.M. Enoka, Detecting the unique representation of motor-unit action potentials in the surface electromyogram, J. Neurophysiol. 100 (3) (2008) 1223–1233, http://dx.doi.org/10.1152/jn.90219.2008.
[12] G.D. Meekins, Y. So, D. Quan, American association of neuromuscular & electrodiagnostic medicine evidenced-based review: Use of surface electromyography in the diagnosis and study of neuromuscular disorders, Muscle Nerve 38 (4) (2008) 1219–1224, http://dx.doi.org/10.1002/mus.21055.
[13] J. Bashford, K. Mills, C. Shaw, The evolving role of surface electromyography in amyotrophic lateral sclerosis: A systematic review, Clin. Neurophysiol. 131 (4) (2020) 942–950, http://dx.doi.org/10.1016/j.clinph.2019.12.007.
[14] M. Hakonen, H. Piitulainen, A. Visala, Current state of digital signal processing in myoelectric interfaces and related applications, Biomed. Signal Process. Control 18 (2015) 334–359.
[15] C. Spiewak, A comprehensive study on EMG feature extraction and classifiers, Open Access J. Biomed. Eng. Biosci. 1 (1) (2018) 17–26, http://dx.doi.org/10.32474/OAJBEB.2018.01.000104.
[16] L.R. Quitadamo, F. Cavrini, L. Sbernini, F. Riillo, L. Bianchi, S. Seri, G. Saggio, Support vector machines to detect physiological patterns for EEG and EMG-based human–computer interaction: a review, J. Neural Eng. 14 (1) (2017) 011001, http://dx.doi.org/10.1088/1741-2552/14/1/011001.
[17] S. Anowarul Fattah, Identifying the motor neuron disease in EMG signal using time and frequency domain features with comparison, Signal Image Process. An Int. J. 3 (2) (2012) 99–114, http://dx.doi.org/10.5121/sipij.2012.3207.
[18] A. Verma, B. Gupta, Detecting neuromuscular disorders using EMG signals based on TQWT features, Augment. Hum. Res. 5 (1) (2020) 8, http://dx.doi.org/10.1007/s41133-019-0020-7.
[19] A. Mokdad, S.M. El Amine Debbal, F. Meziani, Diagnosis of amyotrophic lateral sclerosis (ALS) disorders based on electromyogram (EMG) signal analysis and feature selection, Polish J. Med. Phys. Eng. 26 (3) (2020) 155–160, http://dx.doi.org/10.2478/pjmpe-2020-0018.

[20] N. Sengar, M.K. Dutta, C.M. Travieso, Identification of amyotrophic lateral sclerosis using EMG signals, in: 2017 4th IEEE Uttar Pradesh Sect. Int. Conf. Electr. Comput. Electron. 2018-Janua, IEEE, 2017, pp. 468–471, http://dx.doi.org/10.1109/UPCON.2017.8251093.

[21] P. Zhou, X. Li, F. Jahanmiri-Nezhad, W. Rymer, P.E. Barkhaus, Duration of observation required in detecting fasciculation potentials in amyotrophic lateral sclerosis using high-density surface EMG, J. Neuroeng. Rehabil. 9 (1) (2012) 78, http://dx.doi.org/10.1186/1743-0003-9-78.

[22] A. Tamborska, J. Bashford, A. Wickham, R. Iniesta, U. Masood, C. Cabassi, D. Planinc, E. Hodson-Tole, E. Drakakis, M. Boutelle, K. Mills, C. Shaw, Non-invasive measurement of fasciculation frequency demonstrates diagnostic accuracy in amyotrophic lateral sclerosis, Brain Commun. 2 (2) (2020) 1–9, http://dx.doi.org/10.1093/braincomms/fcaa141.

[23] T. Tuncer, S. Dogan, F. Ertam, A. Subasi, Computational intelligence in surface electromyogram signal classification, in: High Performance Computing for Intelligent Medical Systems, 2021, pp. 1–22, chapter 2.

[24] T. Tuncer, S. Dogan, A. Subasi, Novel finger movement classification method based on multi-centered binary pattern using surface electromyogram signals, Biomed. Signal Process. Control 71 (2022) 103153.

[25] S. Dogan, T. Tuncer, A novel statistical decimal pattern-based surface electromyogram signal classification method using tunable q-factor wavelet transform, Soft Comput. 25 (2) (2021) 1085–1098.

[26] A. Pereira, D. Folgado, F. Nunes, J. Almeida, I. Sousa, Using inertial sensors to evaluate exercise correctness in electromyography-based home rehabilitation systems, in: 2019 IEEE International Symposium on Medical Measurements and Applications, MeMeA, IEEE, 2019, pp. 1–6.

[27] T. Schultz, M. Wand, Modeling coarticulation in EMG-based continuous speech recognition, Speech Commun. 52 (4) (2010) 341–353.

[28] K.M. Fisher, B. Zaaimi, T.L. Williams, S.N. Baker, M.R. Baker, Beta-band intermuscular coherence: a novel biomarker of upper motor neuron dysfunction in motor neuron disease, Brain 135 (9) (2012) 2849–2864.

[29] N.P. Issa, S. Frank, R.P. Roos, B. Soliven, V.L. Towle, K. Rezania, Intermuscular coherence in amyotrophic lateral sclerosis: A preliminary assessment, Muscle Nerve 55 (6) (2017) 862–868.

[30] M. Kefalas, M. Koch, V. Geraedts, H. Wang, M. Tannemaat, T. Back, Automated machine learning for the classification of normal and abnormal electromyography data, in: 2020 IEEE International Conference on Big Data, Big Data, IEEE, Atlanta, GA, USA, 2020, pp. 1176–1185, http://dx.doi.org/10.1109/BigData50022.2020.9377780.

[31] M. Christ, N. Braun, J. Neuffer, A.W. Kempa-Liehr, Time series feature extraction on basis of scalable hypothesis tests (tsfresh – a python package), Neurocomputing 307 (2018) 72–77, http://dx.doi.org/10.1016/j.neucom.2018.03.067.

[32] C. Quintão, R. Vigário, M.M. Santos, A.L. Gomes, M. de Carvalho, S. Pinto, H. Gamboa, Surface electromyography for testing motor dysfunction in amyotrophic lateral sclerosis, Neurophysiol. Clin. (2021) http://dx.doi.org/10.1016/j.neucli.2021.06.001, S098770532100068X.

[33] P. Rong, G.L. Pattee, A multidimensional facial surface EMG analysis for objective assessment of bulbar involvement in amyotrophic lateral sclerosis, Clin. Neurophysiol. 135 (2022) 74–84.

[34] F. Fernandes, I. Barbalho, D. Barros, R. Valentim, C. Teixeira, J. Henriques, P. Gil, M. Dourado Júnior, Biomedical signals and machine learning in amyotrophic lateral sclerosis: a systematic review, BioMed. Eng. OnLine 20 (1) (2021) 61, http://dx.doi.org/10.1186/s12938-021-00896-2.

[35] I. Rodriguez-Carreno, L. Gila-Useros, A. Malanda-Trigueros, Motor unit action potential duration: Measurement and significance, in: Adv. Clin. Neurophysiol., InTech, 2012, http://dx.doi.org/10.5772/50265.

[36] L.A. Green, A. Christie, D.A. Gabriel, Spike shape analysis for the surface and needle electromyographic interference pattern, Biomed. Signal Process. Control 36 (2017) 1–10, http://dx.doi.org/10.1016/j.bspc.2017.03.006.

[37] M. Barandas, D. Folgado, L. Fernandes, S. Santos, M. Abreu, P. Bota, H. Liu, T. Schultz, H. Gamboa, TSFEL: Time series feature extraction library, SoftwareX 11 (2020) 100456, http://dx.doi.org/10.1016/j.softx.2020.100456.

[38] M.M.O.A. dos Santos, Study of the Electromyographic Signal Dynamic Behavior in Amyotrophic Lateral Sclerosis (ALS) Dissertation (Master's), FCT-NOVA, 2014, p. 76.

[39] M.-H. Soriani, C. Desnuelle, Care management in amyotrophic lateral sclerosis, Rev. Neurol. (Paris). 173 (5) (2017) 288–299, http://dx.doi.org/10.1016/j.neurol.2017.03.031.

[40] S. Solnik, P. Rider, K. Steinweg, P. DeVita, T. Hortobágyi, Teager–kaiser energy operator signal conditioning improves EMG onset detection, Eur. J. Appl. Physiol. 110 (3) (2010) 489–498, http://dx.doi.org/10.1007/s00421-010-1521-8.

[41] D. Dumitru, J.C. King, Motor unit action potential duration and muscle length, Muscle Nerve 22 (9) (1999) 1188–1195, http://dx.doi.org/10.1002/(SICI)1097-4598(199909)22:9<1188::AID-MUS4>3.0.CO;2-I.

[42] F. Pedregosa, G. Varoquaux, A. Gramfort, V. Michel, B. Thirion, O. Grisel, M. Blondel, P. Prettenhofer, R. Weiss, V. Dubourg, J. Vanderplas, A. Passos, D. Cournapeau, M. Brucher, M. Perrot, E. Duchesnay, G. Louppe, Scikit-learn: Machine learning in python, J. Mach. Learn. Res. 12 (2012).

[43] L. Fischer, B. Hammer, H. Wersing, Optimal local rejection for classifiers, Neurocomputing 214 (2016) 445–457, http://dx.doi.org/10.1016/j.neucom.2016.06.038.

[44] M. Gromicho, M. Figueiral, H. Uysal, J. Grosskreutz, M. Kuzma-Kozakiewicz, S. Pinto, S. Petri, S. Madeira, M. Swash, M. Carvalho, Spreading in ALS: The relative impact of upper and lower motor neuron involvement, Ann. Clin. Transl. Neurol. 7 (7) (2020) 1181–1192, http://dx.doi.org/10.1002/acn3.51098.

[45] R. Istenič, P.A. Kaplanis, C.S. Pattichis, D. Zazula, Multiscale entropy-based approach to automated surface EMG classification of neuromuscular disorders, Med. Biol. Eng. Comput. 48 (8) (2010) 773–781, http://dx.doi.org/10.1007/s11517-010-0629-7.

[46] C.J. De Luca, A. Adam, R. Wotiz, L.D. Gilmore, S.H. Nawab, Decomposition of surface EMG signals, J. Neurophysiol. 96 (3) (2006) 1646–1657, http://dx.doi.org/10.1152/jn.00009.2006.

[47] K.C. McGill, Z.C. Lateva, H.R. Marateb, EMGLAB: An interactive EMG decomposition program, J. Neurosci. Methods 149 (2) (2005) 121–133, http://dx.doi.org/10.1016/j.jneumeth.2005.05.015.

[48] W. Sun, J. Zhu, Y. Jiang, H. Yokoi, Q. Huang, One-channel surface electromyography decomposition for muscle force estimation, Front. Neurorobot. 12 (MAY) (2018) 1–12, http://dx.doi.org/10.3389/fnbot.2018.00020.

[49] I. Rodríguez, L. Gila, A. Malanda, I.G. Gurtubay, F. Mallor, S. Gómez, J. Navallas, J. Rodríguez, Motor unit action potential duration, I: Variability of manual and automatic measurements, J. Clin. Neurophysiol. 24 (1) (2007) 52–58, http://dx.doi.org/10.1097/01.wnp.0000236606.53923.0d.